coatings

MDPI

Article

A Method for Accelerated Natural Weathering of Wood Subsurface and Its Multilevel Characterization

Anna Sandak [1,2], Jakub Sandak [1,3,*], Marion Noël [4] and Athanasios Dimitriou [5]

1 Wood Modification, InnoRenew CoE, Livade 6, 6310 Izola, Slovenia; anna.sandak@innorenew.eu
2 Faculty of Mathematics, Natural Sciences and Information Technologies, University of Primorska, Glagoljaška 8, 6000 Koper, Slovenia
3 Andrej Marušič Institute, University of Primorska, Titov trg 4, 6000 Koper, Slovenia
4 Institute Materials and Wood Technology, Bern University of Applied Sciences, Solothurnstrasse 102, Postfach 6096, CH-2500 Biel 6, Switzerland; marion@lekolabs.com
5 The BioComposites Centre, Bangor University, Bangor, Gwynedd LL57 2UW, UK; a.dimitriou@bangor.ac.uk
* Correspondence: jakub.sandak@innorenew.eu; Tel.: +386-4028-2959

Abstract: The function of altering weathering factors and degradation mechanisms are essential for understanding the weathering process of materials. The goal of this work was to develop a method for the acceleration of natural weathering and to investigate the molecular, microstructure and macrostructure degradation of wood caused by the process. Tests were performed in the whole month of July, which, according to previous research, is considered as the most severe for weathering of wood micro-sections. Sample appearance was evaluated by colour measurement. Scanning electron microscopy was used for evaluation of the structural integrity and changes in the microstructure of wood morphological components. Changes on the molecular level were assessed by means of FT-IR spectroscopy. Observation of the effects of weathering allowed a better understanding of the degradation process. Typical structural damage, such as cracks on bordered pits and cross-field pits, and, as a consequence, their erosion, revealed the sequence of the degradation process. It was confirmed that earlywood was more susceptible to damage than latewood. Even if the weathering test was conducted for a relatively short time (28 days) the ultra-thin wood samples changed noticeably. The progress of alteration was similar as usually noticed for wood surfaces, but occurred at shorter exposure times. The estimated acceleration factor was ×3, compare to the natural weathering kinetics of wood. The research methodology presented can be used for the determination of the weather dose-response models essential to estimate the future service life performance of timber elements.

Keywords: photodegradation; wood weathering; SEM imaging; FT-IR spectroscopy; thin samples; accelerated natural weathering

Citation: Sandak, A.; Sandak, J.; Noël, M.; Dimitriou, A. A Method for Accelerated Natural Weathering of Wood Subsurface and Its Multilevel Characterization. *Coatings* **2021**, *11*, 126. https://doi.org/10.3390/coatings11020126

Received: 4 January 2021
Accepted: 19 January 2021
Published: 23 January 2021

1. Introduction

Wood as a building material has traditionally been used for different types of load-bearing structures, decking, façades cladding, doors and windows. Wood, due to its versatile character, is often used in both rustic and modern buildings, as well as frequently applied as a material for retrofitting of existing structures. The trend for raising sustainable buildings, in addition to increasing environmental awareness observed nowadays, leads to the reactivation of bio-architecture as an alternative to other construction techniques [1,2]. However, the major limitation for choosing natural wood for external use is the lack of confidence that many architects, designers and customers have towards this material, mostly due to aesthetic preferences. The speed and pattern of the colour change are difficult to predict and are rarely taken into consideration at the early phases of building design [3].

Today's bio-based building materials, even if well characterized from the technical point of view, are often lacking reliable models describing their performance during service life and the operational durability is still a limiting factor in many applications

and environments. Wooden elements often suffer due to mechanical, environmental or biological alterations during their use phase. The most susceptible parts are unprotected surfaces since they are primarily exposed to ageing, weathering or decay.

Weathering is the general term used to define the slow degradation of materials exposed to weather condition [4]. The intensity of weathering depends on timber species, design solution, function of product and finishing technology applied for wood protection and on the specific local conditions. The corrosion rate of wood is low: approximately 6mm per century in the case of European softwood species [4]. In general, the process of wood weathering leads to a slow breaking down of surface fibers, their removal and, in consequence, a roughening of the surface and reduction of the glossiness. Formation of discontinuities on the surface simplify moisture penetration and allow access of wood-decaying biological agents into the material structure. As a result, mechanical performance of the load-bearing members might decrease.

A critical limitation of the state-of-the-art natural weathering procedures is a fact that the test is very long lasting. Diverse approaches for its acceleration were proposed, including amplification of the absorbed radiation by implementing additional solar light focusing optics, scheduled water spraying, temperature control of the sample, or automatic systems for exposing samples that continuously follow the Sun's position. An example of that sophisticated instruments is Equatorial Mount with Mirrors for Acceleration with Water (EMMAQUA) that is commercially available for testing diverse materials [5]. Even though, the amplification of the weathering process is limited, not to mention elevated costs for such complicated equipment and demanding procedure for the test itself. An alternative approach for accelerating the natural weathering of bio-based materials is reported here. The solution is based on the fact that the most affected part of the sample during natural weathering is the sample surface (subsurface) of few hundreds of micrometre thickness. A pilot experiment was designed to prepare wood micro-sections (ultra-thin samples) and to confront the mechanism of changes to the wood due to the action of atmospheric agents occurring in short term. Similar approach had already been used successfully for investigating the resistance of wood against biological corrosion [6], chemical corrosion [7] as well as atmospheric corrosion [8,9]. Use of extra thin samples permits direct investigation of the surface layer and its disintegration due to photochemical or mechanical degradation.

An artificial weathering is an established alternative for testing a material's resistance to deterioration due to climate related factors. The European standard EN 927-6 [10] describes such a method that is frequently used to assess wood coatings. It uses a specially designed device equipped with temperature control, light radiation by means of fluorescent ultraviolet range A (UVA) lamps, water spray and water condensation units. Another, equally common methodology relays on testing weathering resistance by simulating the Sunlight irradiance by means of xenon lamps [11]. Podgorski et al. reported relatively good agreement for the development of cracking when compared to results from natural weathering of coated wood, with the estimated acceleration factor of $\times 5$ [12]. Even a higher acceleration factor of $\times 10$ was identified there for a loss of surface glossiness. Development of cracking was faster in artificial weathering tests due to higher doses of degrading factors provided in shorter cycles but with precisely controlled exposure conditions. Most artificial weathering methods lack biological impacts as well as the influence of dirt that are present in typical exterior exposure environments [13]. Özgenç noticed significant differences in the colour alteration as well as in compression strength along fibres for samples subjected to the natural and artificial weathering conditions [14]. It was demonstrated that the reason for such differences laid in the lack of several minor factors that are not included in the artificial weathering protocols. These factors include air pollution, biological pests, and snow, as well as difference in the spectral composition of light irradiation, nature of the rain-driven wetting, and humidity variations occurring under natural conditions. Similar observations were reported by Ruther and Jelle, where solar radiation and wind-driven rain were identified as the main factor inducing colour changes [15]. However, the surface greying typically observed for the natural wood exposed to exterior conditions is caused

by mould growth and is hardly replicated in up-to-date artificial weathering tests. Outdoor exposed samples become usually darker at the first stage of weathering, to turn in to lighter tones afterward. This is supported by both visual assessment of inspectors as well as by objective spectra/colour measurements. On the contrary, samples exposed to laboratory weathering cycles turn darker to varying extend and do not exhibit initial increase in International Commission on Illumination (CIE) a^* (green–red) and CIE b^* (blue–yellow) values, typical to samples exposed outdoors. In addition, it was found that samples exposed over a longer period to artificial weathering show a form of unnatural bleaching, not present in wood samples exposed to natural weathering [15]. The overall conclusion is, therefore, that even if several advantages of artificial weathering make this an interesting testing methodology, the results from laboratory weathering can hardly be compared to the real outdoor weathering. The reason lays in different mechanisms and kinetics of the material deterioration, which are especially diverse in complex biological composites such as wood.

Several attempts to understand and model wood weathering have been conducted by various researchers. A review published by Brischke and Thelandersson [16] presents an overview on modelling methodologies used for outdoor performance prediction of wood products. According to the authors, dose-response models seem to be most frequently applied, where the changes in any material property are related to the dosage of the relevant environmental causes. In general, solar radiation and wind-driven rain are the two main driving factors influencing wood surface appearance [17]. They entail further internal stresses of bulk material imposed by cyclic wetting and temperature changes. Methodology for determining the weather dose of the building façade was also reported by Thiis et al. [18]. The authors stated that the surface temperature can be very different than the ambient air temperature, especially when the building elevation is exposed to direct sunlight. Therefore, variation of the exterior microclimate is also important for deterioration extent. Access to an extensive data set generated by different types of sensors is indispensable for the development of high-quality numerical models. The attempt for defining an original algorithm for calculation of "the weathering indicator", by merging the multi-sensor data and linking these to the surface performance indicators, was also presented by the authors [19,20].

New knowledge regarding the role of matrix polymers and their interaction on a molecular level permit discovering of complex biological structures [21]. In particular, microscopic and spectroscopic techniques allow better understanding of the ultrastructure of wood, which is a composite of diverse cell types and chemical components acting together to serve the needs of a plant [22]. Tracheids are the major component of softwood. Their cell wall is composed of several layers: middle lamella, primary wall and secondary walls (S1–S3) [23]. The thickness, chemical composition and structure (microfibril orientations) of those layers vary due to their role. Both primary and secondary walls contain pectin, cellulose, and hemicellulose, although in different proportions. The function of the middle lamella is adhesion of adjacent cells. The primary wall consists of a rigid skeleton of cellulose microfibrils. A layered secondary cell wall, composed of lignin, cellulose, and hemicellulose, provides strong mechanical strength [24].

Microstructure analyses of wood investigated by scanning electron microscopy (SEM) were conducted by several researchers. Hamed et al. [25] and Jingran et al. [26] used SEM for monitoring changes in archaeological wood. Nicole et al. [27] and Popescu et al. [28] investigated decayed wood. Singh et al. [29] used light and scanning electron microscopy for visualization of wood impregnation and imaging of the wood–matrix polymer interface in bio-composites [30]. Microscopic structural analyses of weathered wood were conducted by several researchers [31–33]. Ganne-Chédeville et al. [34] used SEM images for the evaluation of wood façade elements after cleaning treatments. SEM is an essential tool allowing observation of the structural changes in degraded wood tissues at the level of cell wall [25]. Even if the obtained information refers mostly morphological and structural changes of the wood, it might also indicate changes in its chemical structure. Spectroscopy

allows even more detailed investigation of chemical composition by revealing molecular structure of wood and functional groups of its constituents [35]. Specific utilization of spectroscopy for the assessment and monitoring of timber members has been proposed by several researchers and an overview was previously presented by the authors [36]. Two-dimensional correlation spectroscopy (2D-COS) used for the analysis of spectral data allowed the identification of small and weak peaks that are masked in one-dimensional spectrum by highlighting spectral changes caused by external disturbances (exposure time). The method was previously used for the evaluation of the degradation stage of wood [37], evaluation of heat-treated wood [38] or wood species discrimination [39].

The goal of this research was to investigate the feasibility of the novel approach for accelerated natural weathering of wood. An extent of the microstructure degradation and other alterations on the molecular, microscopic, and macroscopic levels recorded in ultra-thin wood samples were confronted with thick references. As a result, an acceleration factor relating weathering kinetics of ultra-thin samples with references was estimated. An additional objective was to develop a novel testing protocol resulting in at least comparable or even more detailed characterization with simplified sample preparation, but still assuring significant shortening of the natural weathering procedure.

2. Materials and Methods

2.1. Experimental Samples

Experimental samples were prepared from Norway spruce wood (*Picea abies* L. Karst.) originated from Italian Dolomite mountains (Trentino Region, Italy). A single log 0.5 m long, extracted from the bottom part of the trunk was spitted to assure radial surface opening. A board 30 mm × 50 mm × 500 mm (radial × tangential × longitudinal directions respectively) was cut out from the sapwood assuring defect free and uniform yearly ring structure. The average yearly ring width was 1.9 mm and latewood width 0.8 mm. No drying process was used to minimize wood properties alteration due to elevated temperature. Wet board was finally processed on the slicing planner (Super MECA-S, Marunaka Tekkonsho Inc., Shizuoka, Japan) to prepare ultra-thin experimental samples. This method allowed the preparation of a high number of defect-free specimens from a limited source of material, minimizing natural heterogeneity of biological material. Moreover, samples prepared in this way might be immediately characterized after weathering (e.g., direct SEM observation or spectroscopic measurement in transmission mode) without supplementary interference (e.g., microtome sectioning), which might affect their original state [40]. The thickness of samples was ~100 µm and the efficient surface exposed to weathering was 30 mm × 30 mm (width × length).

An additional set of reference (thick) samples was prepared from the same log as ultra-thin samples to assure minimal variance of the tested wood properties. Twelve wooden blocks of dimensions 30 mm × 10 mm × 50 mm were extracted and used for natural weathering.

2.2. Weathering Test

Sets of both ultra-thin and thick samples (Figure 1b) were placed for natural exposure at 45° to the horizon, facing four cardinal directions: north, west, east and south in San Michele, Italy (46°11′15″ N, 11°08′00″ E, 206 m above sea level). The sample stand (Figure 1a) was installed on the roof of the building assuring no shadowing of surrounding structures and vegetation. The test was carried out from July 2014 to June 2015. Ultra-thin samples were collected before exposition (0) and after 1, 2, 4, 7, 9, 11, 14, 17, 21, 24 and 28 days of natural weathering. Thick samples were collected once per month for a duration of one year. The weather data observed during the test are summarized in Table 1. In addition, the early climate data for exposure location are provided in Table 2. Experimental samples together with non-weathered references were conditioned after collection in the dark climatic chamber (20 °C, 60% Relative Humidity (RH)) to the equilibrium moisture content of ~12%.

(**a**) (**b**)

Figure 1. Experimental stand (**a**) and set of ultra-thin and thick wood samples (**b**) exposed to natural weathering in San Michele All'Adige (Italy).

Table 1. Weather data acquired during weathering progress of ultra-thin samples.

Day of Exposure	0	1	2	4	7	9	11	14	17	21	24	28
Mean temp (°C)	–	18	20	22	17	18	20	22	24	20	21	19
∑ radiation (MJ/m^2)	–	30	60	105	162	202	251	324	407	469	527	581
∑ insolation (h)	–	14	26	46	70	90	108	139	173	202	229	255
total rain (mm)	–	11	0	2	43	0	2	0	0	0	0	13
RH (%)	–	84	59	73	93	68	68	68	60	80	70	89
mean wind speed (m/s)	–	0.8	1.9	0.5	0.5	0.9	1.2	0.9	1.0	0.1	0.8	0.5

Table 2. Weather data acquired during weathering progress of reference (thick) samples.

Month	July	August	September	October	November	December	January	February	March	April	May	June
Mean temp (°C)	19	17	10	6	4	1	−4	−2	0	6	8	13
RH (%)	68	69	77	83	71	76	84	84	79	76	76	78
Wind speed (m/s)	0.6	0.5	0.4	0.3	1.0	1.0	0.9	0.4	0.4	0.7	0.3	0.6
Wind direction (°)	199	165	159	62	333	338	317	337	1	187	168	185
∑ rainfall (kg/m^2)	99	176	147	192	4	2	26	61	21	115	237	312
∑ snowfall (kg/m^2)	0	1	8	24	11	1	25	102	81	29	16	8
∑ irradiation (kWh/m^2)	195	175	126	87	68	54	55	70	134	157	179	171

2.3. Macroscopic Observation: Colour Measurement

Sample colour was measured by using ultraviolet-visible-near infrared (UV–VIS–NIR) spectrometer Maya2000pro, produced by Ocean Optics (Largo, FL, USA). Equipment calibration was carried out using white and black standards provided by the manufacturer. Changes in colour were also assessed by a colorimeter following the CIE *L*a*b** system where colour is expressed as three coordinates: *L** (lightness), *a** (red-green tone) and *b** (yellow-blue tone). CIE *L*a*b** colours were measured using MicroFlash 200D spectrophotometer (DataColor Int, Lawrenceville, NJ, USA). The selected illuminant was D65 and viewer angle was 10°. All specimens were measured on three different spots over the weathered surface. Digital images of sample surfaces were also captured on an G2710 (Hewlett-Packard, Palo Alto, CA, USA) office scanner, in parallel to the colour measurements.

2.4. Microscopic Observation: Scanning Electron Microscopy

Small pieces of investigated samples were cut out and glued with carbon tape sticker to the sample holder. The samples were placed in SC7620 (Quorum Technologies, Laughton, UK) Mini Sputter Coater/Glow Discharge System device and then plasma coated for 90 s

with 10 nm gold/palladium (Au/Pd) layer. Prepared samples were investigated by using TM 3030 (Hitachi, Tokyo, Japan) Scanning Electron Microscope (SEM). An acceleration voltage of 15 kV was used for imaging of samples. Images were acquired with a dedicated software provided by the equipment producer.

2.5. Molecular Observation: Fourier Transform–Infra Red Measurement

All experimental samples were measured with an Alpha Fourier transform infrared (FT-IR) spectrometer produced by Bruker Optics GmbH (Ettlingen, Germany) equipped with universal sampling module allowing measurement in transmission. The spectral range measured was between 4000 and 600 cm^{-1}. The spectral resolution of the spectrophotometer was 4 cm^{-1}; each spectrum has been computed as an average of 32 successive measurements in order to minimize the measurement error. Three measurements were performed on each sample. Opus 6.5 (Bruker, Ettlingen, Germany), PLS_Toolbox (Eigenvector Inc, Manson, IA, USA), available as an extension of the Matlab package (Mathworks Inc, Natick, MA, USA) and LabView 2019 (National Instruments Inc, Austin, TX, USA) software packages were used for spectral pre-processing and data mining. IR spectra before interpretation were corrected by extended multiplicative scatter correction (EMSC). EMSC was applied to minimize an effect of nonuniform optical density for measured wood specimens and related differences in the measured amplitude and baseline deviation [41]. Three replicate measurements on each sample were averaged and the resulting spectrum was baseline-corrected. A lot of research efforts have been directed toward systematizing the infrared peaks interpretations that resulted in several scientific publications [42–47]. These papers were an inspiration to review the available know-how and adopt it for the specific needs of this research (wood weathering). The complete list of peaks observed in investigated experimental specimens is summarized in Table 3.

Table 3. Band assignment for FT-IR transmittance spectra of Norway spruce [42–47].

Number	Peak Position	Band Assignment
1	985	CO valence vibrations
2	1024	CO stretching in cellulose and non-cellulose polysaccharides
3	1060	C–O + C–C stretch of cellulose
4	1110	Aromatic skeletal; C–C stretch
5	1160	CO stretching in ester groups in lignin
6	1201	untreated cellulose (ρ OH; δ CH)
7	1226	syringil ring; C–O stretching lignin and xylan
8	1265	guaiacyl ring vibrations and CO stretching lignin
9	1315	C–H vibration in cellulose; C–O in syringil derivatives
10	1334	vibration in CH and stretching in CO related to syringil ring
11	1370	CH bending in cellulose and non-cellulosic polysaccharides
12	1425	vibration of aromatic structures in lignin
13	1452	aromatic skeletal vibrations of lignin and CH_2 vibration in cellulose
14	1508	aromatic skeletal vibrations of lignin and C=O stretching
15	1598	aromatic skeletal vibrations of lignin and C=O stretching
16	1652	stretching vibrations of conjugated C=O
17	1732	C=O–OH stretching in glucuronic acid in xylan
18	2902	symmetric CH_2 valence vibrations
19	2940	asymmetric stretching vibrations of CH related to methyl and methylene in lignin, cellulose and hemicellulose
20	3149	–OH stretching in cellulose
21	3280	C–H stretching in methyl and methylene groups
22	3375	–O(3)H O(5) intramolecular hydrogen bonds in cellulose
23	3496	moderately H-bonded water
24	3565	valence vibration of H bonded OH groups
25	3602	weakly H-bonded water

Standard spectra interpretation was aided by two-dimensional spectra correlation (2DCOS), which permits direct deconvolution and determination of correlations between bands in the spectra; 2D-IR spectroscopy allows new information to be obtained, which cannot be acquired by using conventional IR and its derivative spectra. The algorithm proposed by Noda [48] was implemented for the needs of this research. All spectra were

interpolated before analysis in order to compensate uneven exposure time, considered here as the 2DCOS disturbance factor.

3. Results

3.1. Macroscopic Level

The appearance of investigated samples after natural weathering in diverse exposure times is presented in Figure 2. The changes in colour are observed in parallel with samples disintegration evident from day 17. Samples become yellowish with the progress of degradation. It is noticed that weathering caused removal of wood fibers, presence of cracks and increase in brittleness of samples.

Figure 2. Appearance changes of ultra-thin (**a**) and reference thick (**b**) wood samples exposed to natural weathering in San Michele All'Adige (Italy). Note: arrow indicate weathering-induced damages to wood cells.

Visible range reflectance spectra of the test samples in this study shows that spruce tends to darken with weathering time, as shown by a decrease of the reflectance value (Figure 3). The reflectance value dropped after one day of exposure. Further changes, as observed after day 7 until the end of the experiment, were more consistent and resulted in a nearly constant VIS spectrum after three weeks of weathering. Analogous results were obtained by measurement of colour with colorimeter. The CIE $L^*a^*b^*$ colour coordinates system is widely used to represent colours in three-dimensional space. According to the CIE Lab definition, L^* represents lightness (varying from 100-white, to 0-black). Similarly, a^* and b^* are chromaticity coordinates, where $+a^*/-a^*$ corresponds to red/green, and $+b^*/-b^*$ to yellow/blue tonality. A decrease of L^* was observed for all exposure directions (Figure 4). The value of a^* increased in the first days of exposure and from day 4 seems to be stable. The noticeable increase in b^*

value, visible as yellowing of wood, is also observed for all exposure directions; however, it is followed by *b** values drop after one week of exposure.

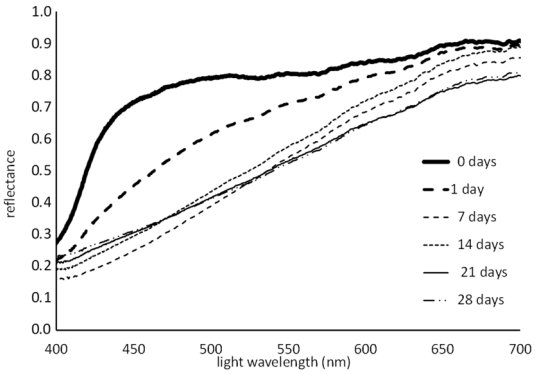

Figure 3. Reflectance VIS spectra of the wood exposed to natural weathering.

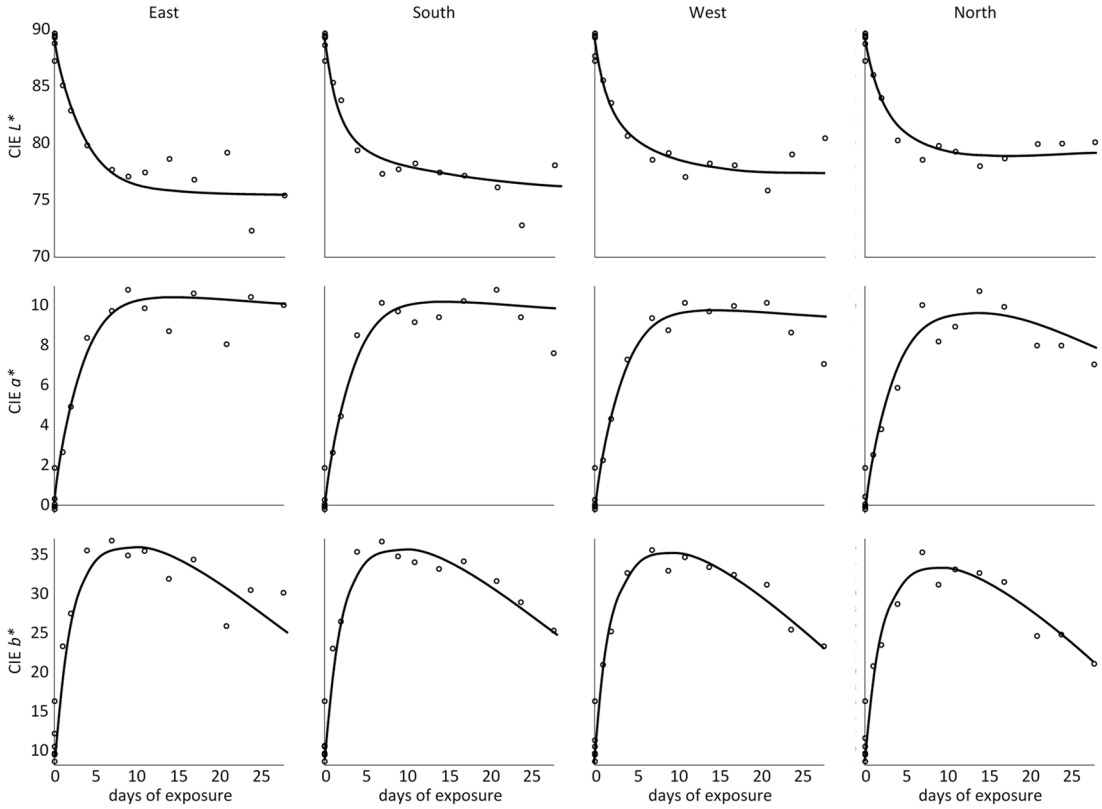

Figure 4. Change of CIE *L*a*b** colour coordinates in ultra-thin wood samples exposed to natural weathering.

3.2. Cellular Level

The first sign of deterioration visible on the SEM images was openings of bordered pits membranes (torus) in radial walls of earlywood tracheids (Figure 5a). In the successive step, the membrane covering the piths was broken (Figure 5b) and presence of small diagonally oriented micro-checks was observed (Figure 5c). With the progress of degradation, an enlargement of the pith crack was noticed as a result of contraction of the cell wall caused by moisture variation (Figure 5d).

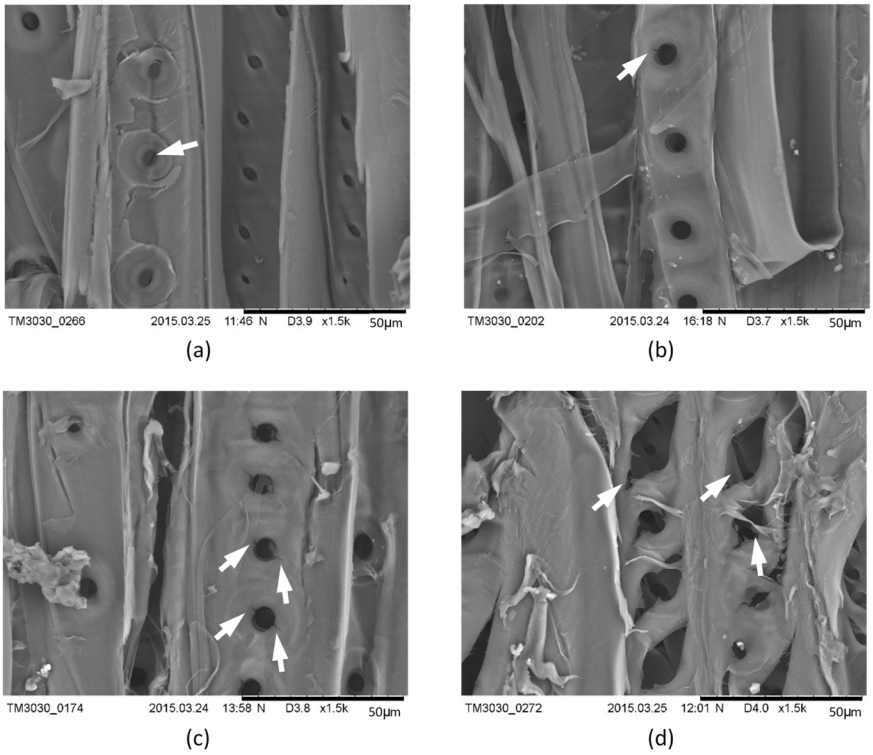

Figure 5. SEM images of earlywood exposed to the south for 2 days (**a**), 7 days (**b**), 9 days (**c**) and 21 days (**d**). Note: arrow indicate weathering-induced damages to wood cells.

Evidence of fungal infection (not visible by naked eye) was found after 17 days of natural exposure, indicating that the growth of microorganisms begins by deposit of their spores into the micro-cracks. Evaluation of the earlywood zones of samples exposed to four directions after 9 days proved that the degradation kinetics vary according to exposure direction. The experimental samples images at the final stage (day 28) are shown in Figure 6, which presents SEM images of latewood zone. Cracks propagate through the cell wall along the progress of decomposition. Pits are completely eroded, and the degradation products are continuously removed with rain. However, the northern samples seem to be relatively less affected by the weathering process (Figure 6c). The time-related progress of morphological changes of the investigated samples is systematically presented in Figure 7.

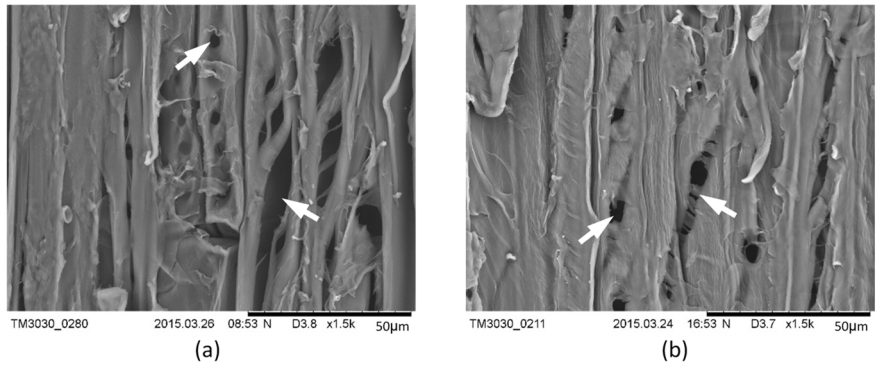

Figure 6. *Cont*.

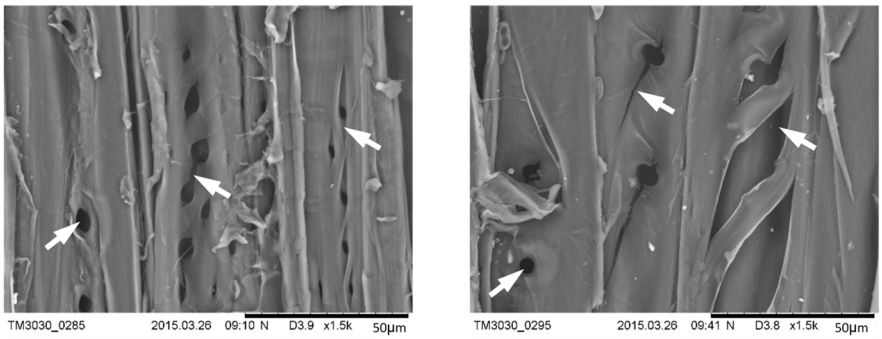

Figure 6. SEM images of latewood exposed to different exposure sites: south (**a**), west (**b**), north (**c**) and east (**d**). Note: arrows indicate weathering-induced damage to wood cells.

Day of exposure		0	1	2	4	7	9	11	14	17	21	24	28	
spores deposition	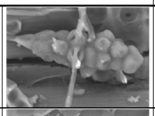	×	×	×	×	×	×	×	×	·	·	·	●	× - no · - seldom ● - intense
degraded surface	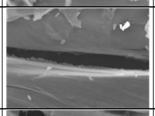	×	×	×	×	·	·	·	·	·	●	●	●	× - no · - little ● - very
big cracks in cell wall	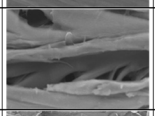	×	×	×	×	×	×	×	·	·	●	●	●	× - no · - some ● - many
diagonally oriented micro-checks in cell wall	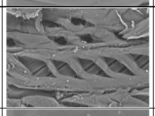	×	×	×	×	●	●	●	●	●	●	●	●	× - no ● - yes
dust deposition	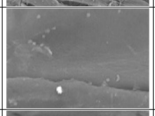	×	×	·	·	·	·	·	●	●	●	●	●	× - no · - some ● - intense
cell wall delamination	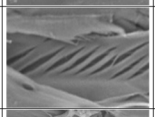	×	×	×	·	·	·	·	·	●	●	●	●	× - no · - some ● - intense
border piths crack	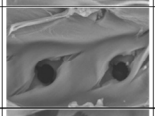	×	×	×	·	·	·	·	●	●	●	●	●	× - no · - seldom ● - all
border piths broken membrane	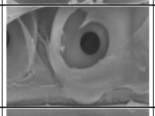	×	×	×	×	●	●	●	●	●	●	●	●	× - no ● - yes
border piths opening membrane	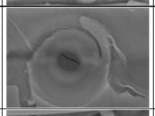	×	×	●	●	●	●	●	●	●	●	●	●	× - no ● - yes
cross field pits crack	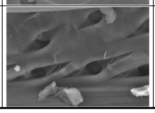	×	×	×	×	×	×	×	×	·	·	●	●	× - no · - present ● - large

Figure 7. Microscopic observation for samples exposed to natural weathering for the south direction.

3.3. Molecular Level

FT-IR spectra measured in transmission mode on samples at various stages of degradation clearly show the progress of changes related to functional groups of wood polymers (Figure 8). The band assignment (Table 1) allowed the identification of 25 peaks that might

be observed and interpreted. The most evident are changes in spectra intensity of bands #7, #8, #14 assigned to aromatic skeletal vibrations of lignin. In all the above-mentioned peaks, the intensity diminishes with weathering progress, consequently, the peaks disappear, indicating decomposition of corresponding chemical component (or functional group). The region 3900–2700 cm^{-1} reflects essentially the amounts and structure of hydroxyl groups in various types of hydrogen bonding of wood components [44]. Even if bands assigned to hydroxyl groups in IR spectrum are better resolved after deconvolution, changes noticed in #24 and #25 reflect reduction in hygroscopic properties of wood exposed to the weathering process [43].

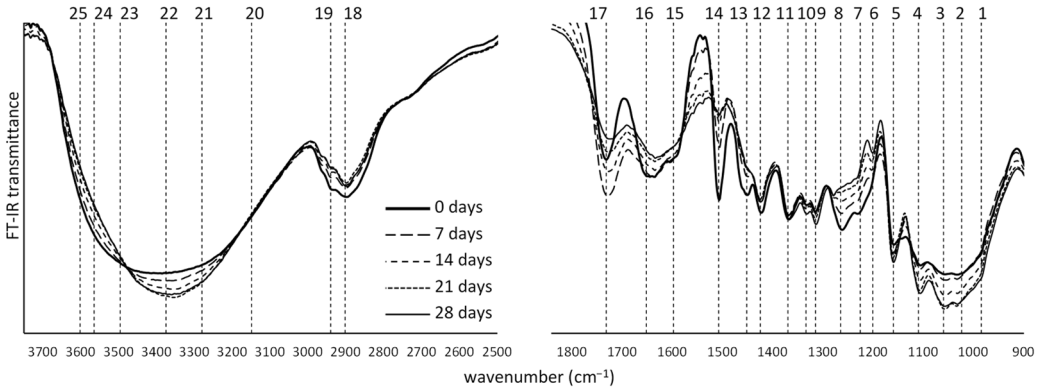

Figure 8. Changes to FT-IR transmittance spectra of Norway spruce wood due to southern exposure to natural weathering.

Peak #14, assigned to aromatic skeletal vibrations of lignin and C=O stretching, was selected to illustrate changes of its intensity due to weathering progress in different cardinal directions (Figure 9). In general, similar progress of intensity changes can be observed; however, the deviations are slightly less intense in the case of samples exposure to north compared with other directions. It is especially evident in the last week of exposure, where intensity of degradation is apparently lower than in the other three cardinal directions. For southern exposure, the highest changes are observed at the initial stage (up to first two weeks), followed by less intense variation in the second part of the experiment. Eastern exposure seems to follow the southern; however, after 14 days, the intensity is less pronounced. Western exposure is less affected up to three weeks. After that period, both (western and eastern) exposures reach the same degradation level as south.

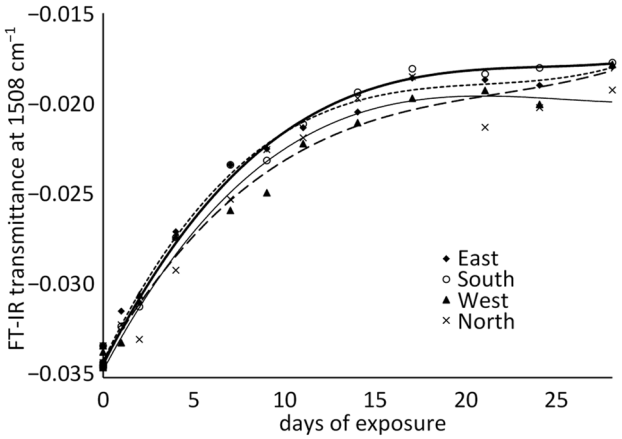

Figure 9. Changes to FT-IR lignin peak (1508 cm^{-1}) along the natural weathering test duration in samples exposed to diverse cardinal directions.

Two-dimensional correlation spectroscopy (2D-COS) was developed by Noda and involved a series of spectra being recorded from one or more samples during or following

perturbation [48]. The resulting spectral data matrix allowed identification of compositional differences within and between samples. Changes in data are visualized in 2D spectral maps. Correlations between measured variables is included in the synchronous matrix. The asynchronous matrix represents sequential variations occurring in the data. The peaks might be located on the diagonal or off the diagonal space. Peaks located on the diagonal (autopeaks) show regions of the spectrum that are changing with respect to the average spectrum of the series. Peaks off the diagonal (cross peaks) show the correlation intensity (positive or negative) of different bands [48].

Figure 10 presents homospectral correlation, where two identical assemblies of data (spectra) are used. The synchronous 2D IR correlation spectrum shows strong positive autopeak at #14. The magnitude of autopeak corresponds to the overall extent of spectral intensity variation observed for specific wavenumber. Presence of other regions assigned to functional groups in lignin (#12, #13 and #15) indicated changes in intensity during weathering progress, meaning that they are susceptible to external perturbation. In fact, the changes in intensity of peak #14 as observed on Figure 8 are very evident. Positive peaks are highlighted by red colour, in contrast to negative peaks marked in violet. The positive peak on the synchronous spectrum indicates that spectral bands corresponding to coordinates of that peak change continuously in the way that direction of changes (increase or decrease) is identical for both wavelengths. Conversely, the negative peak appears when one wavelength increases, while the second wavelength decreases. The sign of asynchronous spectrum allows identification the sequence of changes occurring at both confronted wavelengths [49]. Crosspeak at coordinates 17–14 represent negative intensity. It indicates that changes of the intensity of both bands are substantially different (aromatic skeletal vibrations of lignin and C=O stretching versus C=O–OH stretching in glucuronic acid in xylan).

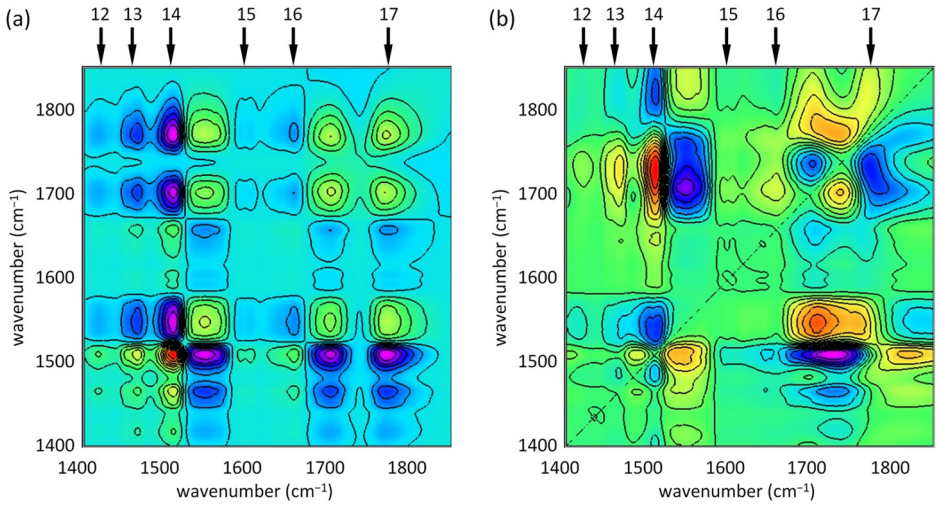

Figure 10. 2D spectral correlation of the FT-IR spectra of Norway spruce wood exposed to south direction in San Michele All'Adige (Italy): (**a**) synchronous spectrum; (**b**) asynchronous spectrum

4. Discussion

According to Raczkowski [9], changes in wood structure, caused by natural weathering and expressed by the reduction in tensile strength, are more intensive during the summer months in comparison with autumn and winter; therefore, our tests were carried out in July. During the weathering experiment, the mean temperature oscillated around 20 °C, while relative humidity was slightly above 70%. Table 1 contains meteorological data captured during sample exposure. Three major rain events and an additional two days with small (2 mm) precipitation were observed. The total hours of insolation were 255, accounting for 581 MJ/m^2. The test duration was limited to 28 days; however, according to Evans [50], the weathering conditions in 45° south exposure are accelerated relative

to vertically installed elements. The configuration of experimental samples (~100 µm thickness of strips) allowed their non-destructive and direct analysis with several methods, such as IR spectroscopy in transmission mode or SEM observation without microtome sectioning. Changes in surface texture, colour and chemical composition being an overall result of exposure to various environmental conditions such as moisture, heat and solar radiation were assessed at different levels providing a wide range information regarding degradation process.

The relatively short exposure time affected appearance of investigated wood. Yellowing of the wood is caused by the formation of chromophoric groups of secondary origin [51,52]. When the chromophoric groups leach from the wood, the wood colour changes further, eventually converting to grey shades. Due to limitation of experiment to one month, this phenomenon was not observed within this research. Analogous results regarding colour changes of wood due to weathering was reported previously by authors while performing artificial weathering test according to EN 927-6 [53]. The changes in colour were already evident after 28 h of artificial weathering. Specific shape of curves representing colour coordinates (CIE b^* measured for all cardinal direction and CIE a^* measured for north) disqualify their use for modelling general trends in the appearance change (Figure 4). In fact, wood might have similar colour values after receiving different weathering doses (e.g., CIE b^* of samples exposed for one and four weeks). The pattern of initial increase of CIE b^*, followed by its decrease, was also reported by other authors [51,54,55]. It was explained by lignin degradation and photooxidation of $–CH_2$ and –CH(OH) groups, with the formation of secondary chromophoric structures (quinones).

Microscopic methods provide detailed information about surface morphology. Scanning electron microscopy is considered a valuable tool for the examination of the morphological characteristics of degraded wood at the level of cell wall, evaluating their damage and detecting eventual presence of decay [25]. As stated by Turkulin [56], observation of the effects caused by photo degradation may provide information about structural integrity of wood surface and help understanding the weathering process. The process of thin wood section destruction due to natural weathering was previously investigated by Raczkowski [9]. He stated that the degradation penetrates relatively deep and observed that the decrease of mechanical strength properties is very significant. According to Turkulin et al. [31], a weathered wood surface shows damage to several anatomical elements: development of cracks of bordered pits, presence of cracks and loss of membranes of the ray pits, and expansion of cracks that can be seen on the lumen surfaces, originating at single pits (Figure 5). Thinning of the cell walls is due to breakdown of lignin in the S2 layer of the cell wall [56]. Progress of weathering (UV degradation, leaching effect of water and mechanical damages caused by wind blow) leads to extensive destruction of the pit membrane and further crack propagation (Figure 5d). Pit openings are then enlarged and, in consequence, the whole pit erodes away. According to Sandberg [57], the orientation of these cracks suggests that these follow the fibril orientation in the S2-layer of the cell wall. Pandley and Pitman [58] reported that specific ridges on the S3 wall layer, wall checking, pit degradation and middle lamella breakdown are typical microscopic features characteristic for natural wood exposed to weathering.

Fungal infestation of investigated samples was noticed after the third week of exposure. Turkulin [56] observed first spores after only 4 days of exposure; however, more intense fungal growth was noticed by him after 41 days. In general, fungal development is constrained on the surfaces exposed to high sun radiation; therefore, intense UV absorbance slows down speed of colonization by fungi. However, summer 2014 was rainy and relatively cooler than usual. Consequently, it promoted growth of the fungi, even on samples with southern exposure. Owen et al. [59] observed that degradation caused by the combined weathering stimuli, including both UV light and precipitation, is considerably more intensive and rapid than exposure to each parameter separately. UV radiation leads to lignin decomposition (photolysis) and, in consequence, to delamination of surface fibres. In particular, the chromophoric groups of lignin are strong UV absorbers and responsible

for yellowing of the surface [51]. The other apparent result of the intensive delignification process is brittleness of the samples. Degradation of lignin was also observed while analyzing IR spectra. The most pronounced reduction of intensity was evident for band #14 and is related to degradation of lignin caused by UV radiation. Similar statements were derived by other researchers [51,60], who observed a decrease of peaks assigned to the lignin along the irradiation time in laboratory experiments. Lignin and extractives are considered as absorbers of UV radiation; therefore, these components suffer major degradation. When the sample system is under an external perturbation, various chemical constituents of the system are selectively excited, and the degrees and orders of the excitations are different [61]. In our case, weathering progress being external perturbation in the system affects molecular structure of investigated material. 2DCOS reveals characteristic behaviours of individual molecular constituents, in particular lignin susceptible to weathering process. Since the intensity of peaks on the autocorrelation spectrum is directly proportional to the relative importance of the intensity change in the original spectra, it can be stated that aromatic skeletal vibrations of lignin are the most vulnerable functional groups.

The observation of weathering process on three different scales, macroscopic, microscopic and molecular, allowed comparison of mechanisms occurring on various levels. It was assumed that the southern location might cause slightly more degradation of wooden surfaces, even in a relatively short time. It was related to longer exposure of UV radiation and, in consequence, more rapid changes of surface moisture. Northern location seems to be less susceptible to degradation, especially at the beginning of weathering. It corresponds to changes of integrated cumulative solar radiation (SR) calculated according to the method proposed by Grossman [62]. It can be clearly seen that the value of cumulative SR of southern exposure is double than northern (80 and 40 $kW \cdot m^{-2}$, respectively) [63]. This phenomenon might explain variation in weathering intensity between exposure sites.

The use of ultra-thin wood samples for investigation of material resistance to natural weathering as reported here reveals that mechanism of degradation as well as sequence of material deterioration follows directly state-of-the-art understanding of wood weathering processes. Investigation of the effect of natural weathering on the microstructure of radiata pine by means of SEM shows analogous deterioration sequence. Degradation of the pit membranes was followed by the gradual enlargement of the pit aperture to the approximate limit of the pit chamber, development of microchecks in the pit borders and to ultimate destruction of pit borders in earlywood tracheids in about 6 months [64].

The particular sample geometry (ultra-thin thickness) determined elevated kinetics of such changes and shortened response time of the material for the weather dose. Analogous approach was proposed by Wang et al. for other types of materials [65]. Their study was related to the thickness-dependent accelerated ageing method that leaded to the more severe ageing degree of the thinner specimens. The phenomenon was explained by the ratio of aged area to the total area. It was reported that in the thinner specimens the ratio was larger than in the thicker specimens. It is always a challenge to determine a specific quantifier of the weathering acceleration factor (AF). Jelle proposed calculation of AF by comparing natural and artificial weathering [66]. He assumed that the higher UV intensity (W/m^2) and total energy (kWh/m^2) in the weathering apparatus is proportional to the aging process. However, the natural weathering process is more complex, as includes several other than UV irradiation factors influencing the degradation rate [67]. This might be a reason to the wide array of reported AF values, ranging between 5 to 250, while comparing the laboratory results with outdoor tests in natural climate.

For the needs of this research a direct comparison approach was implemented by confronting above presented results with corresponding characterizations for thick wood samples (10 mm thickness) made of the same wood piece. A set of such thick samples was exposed during the natural weathering test in vicinity of thin samples. In that case, weathered samples were collected from the stand for duration of one year, one sample each lunar month. "Thick" samples were assessed with same analytical techniques as ultra-thin strips, by applying necessary amendments (such as Attenuated Total Reflectance (ATR) instead of

transmission mode of infrared spectrometer, or reflectance instead of transflectance when measuring colour spectrum). The trends of material changes can be then directly compared between thin and thick wood samples to understand the weathering process acceleration. Assuming that the sole difference between both sample types is kinetics of deterioration, it become possible to identify an acceleration factor. This factor was determined empirically by adjusting the time scale for diverse deterioration kinetics curves measured on ultra-thin and thick samples to assure an overlap of both trends. An example of such analysis is presented in Figure 11 where acceleration factor of $\times 3$ was applied for the CIE *L* and CIE *a* colour curves in combination with the lignin deterioration trends at peak #14 (1507 cm^{-1}). The numerical factor (determined through visual observations) can be therefore used to quantify the time relation between both confronted natural weathering configurations. It is clear that such an approach introduces certain over-simplification as nature of scanned parameters is different, as well as the weather dose distribution is very different during periods of one month (thin samples) and one year (thick samples). In any case, it provides a scientific basis for a statement that the use of ultra-thin samples for natural weathering may lead to shorten the test duration still preserving the complex physical and chemical mechanism of the material, particularly surface, deterioration when exposed to natural weather conditions.

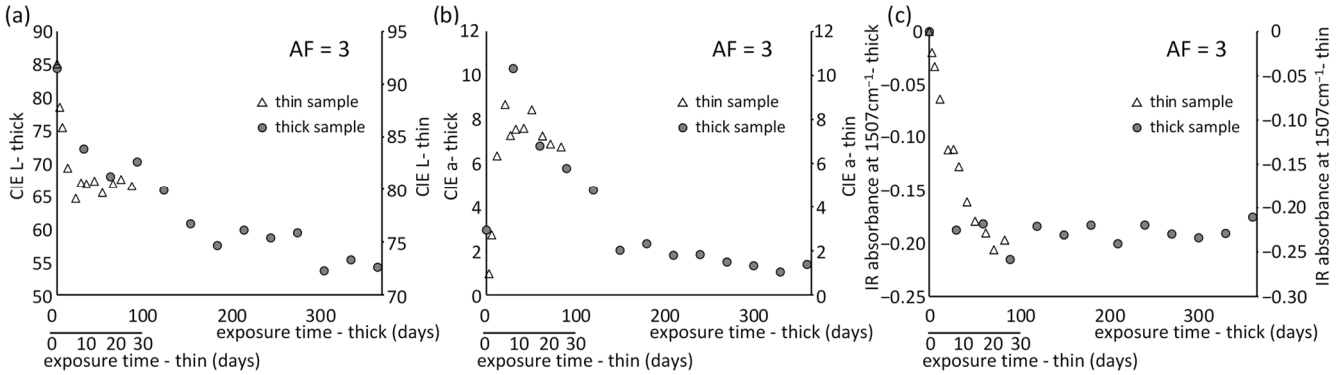

Figure 11. Confrontation of (**a**) CIE *L*, (**b**) CIE *a* and (**c**) lignin peak #14 of IR spectrum deterioration kinetics curves for experimental data acquired from thin and thick wood samples exposed to natural weathering, assuming acceleration factor AF = 3.

An important limitation of using ultra-thin samples for natural weathering testing is a fact of losing a complex interaction of different layers within material bulk. It implicates a dramatic change to the diffusion of moisture and heat within bulk material. However, in the context of the wood weathering it is clear that the most relevant changes occur in the subsurface of the material. The majority of extensive chemical–physical reactions (photolysis, hydrolysis, etc.), deposition of biological and abiotic agents, as well as moisture induced deformations take place on the surface of sample and progress into bulk interior only after erosion of the external layers. The electromagnetic radiation in the range of photodegrading UV light penetrates wood to the extent of 50–100 μm, that corresponds to the thickness of samples used in this research. Other important missing aspect in the proposed "accelerated natural weathering" approach is a fact that an ultra-thin sample is missing the mechanical support of the bulk. The support constrains moisture-induced deformations and serves as a physical barrier (or buffer) slowing down the moisture and heat transfer. It affects also the number and extend of microcracks formation. Despite the above limitations, using ultra-thin wood samples is a correct approach for assuring replication of the real mechanisms of the weathering occurring in "thick samples". That cannot be assured in alternative up-to-date artificial weathering methods.

5. Conclusions

Understanding the mechanisms of weathering and the role of altering factors is fundamental to assess the actual conditions of timber structures. It is also essential for future performance, and, possibly, to ensure long-term preservation and maintenance. Even if it is impossible to fully integrate results obtained by assessment of thin wood samples with standard wooden samples, the presented approach allowed rapid and reliable assessment of the complex chemical and structural changes occurring within the surface layers.

With the progress of degradation, samples become yellowish. Weathering also caused removal of wood fibers, presence of cracks and, an increase in brittleness of samples. Spectroscopic analysis provided information regarding susceptibility of functional groups to natural weathering. Gradual changes in absorbance intensity of CH deformation of aromatic skeletal vibration of lignin confirmed the vulnerability of this component to photodegradation. Scanning electron microscopy (SEM) was used here for examination of the morphological characteristics of naturally weathered thin wooden samples. The structural degradation was initiated from openings of bordered pits membranes in radial walls of earlywood tracheids. In the following steps, the membrane covering the piths was broken and diagonally oriented micro-checks were observed. The progress of weathering led to entire destruction of the pit membrane and whole pit erosion.

It was confirmed that earlywood was more susceptible to damage than latewood, which was explained by the fact that cells in earlywood have thinner and weaker walls and, in consequence, lower density. It was also observed that western and northern exposure sites are slightly less affected by weathering. First signs of fungal infestation, not visible by naked eye, were observed in the third week of natural weathering.

Even if the weathering test was conducted for a relatively short time (28 days), the progress of ultra-thin wood sample alteration was similar as usually noticed for thick wood surfaces. However, such an extent of changes occurred at shorter exposure times. The estimated acceleration factor was $\times 3$. The research methodology presented here can be directly used for determining the weather dose-response models essential to predict the future service life performance of timber elements. It may also serve as a screening technique for a rapid estimate of the material's resistance to deterioration. In that case, all the natural weathering factors are fully considered, in contrast to artificial weathering procedures limiting the real exposure conditions.

Author Contributions: Conceptualization: A.S., J.S., M.N., and A.D.; methodology: A.S., J.S., M.N., and A.D.; software: J.S.; validation: A.S., J.S., and M.N.; formal analysis: A.S.; investigation: A.S., J.S., M.N., and A.D.; resources: A.S. and J.S.; data curation: J.S. and A.S.; visualization: J.S.; supervision: J.S. and A.S.; project administration: A.S.; funding acquisition: A.S., J.S., M.N., and A.D. All authors have read and agreed to the published version of the manuscript.

Funding: The authors gratefully acknowledge the European Commission for funding the InnoRenew project (Grant agreement #739574 under the Horizon2020 Widespread-Teaming program) and the Republic of Slovenia (investment funding of the Republic of Slovenia and the European Union European Regional Development Fund) and infrastructural ARRS program IO-0035. Part of this work was conducted during project Archi-BIO (BI/US-20-054) funded by ARRS and CLICK DESIGN "Delivering fingertip knowledge to enable service life performance specification of wood"–(No. 773324) supported under the umbrella of ERA-NET Cofund ForestValue by the Ministry of Education, Science and Sport of the Republic of Slovenia. ForestValue has received funding from the European Union's Horizon 2020 research and innovation programme.

Institutional Review Board Statement: Not applicable.

Informed Consent Statement: Not applicable.

Data Availability Statement: The data presented in this study are available on request from the corresponding author.

Acknowledgments: The experimental samples were prepared and weathered during Round Robin test of COST FP1006. The support of COST FP1303 for funding Short Term Scientific Mission of Anna

Sandak is highly acknowledged. Authors would also like to thank Thomas Volkmer for inspiring discussion.

Conflicts of Interest: The authors declare no conflict of interest.

References

1. Ivanović-Šekularac, J.; Čikić-Tovarović, J.; Šekularac, N. Application of wood as an element of façade cladding in construction and reconstruction of architectural objects to improve their energy efficiency. *Energy Build.* **2016**, *115*, 85–93. [CrossRef]
2. De Vetter, L.; Cnudde, V.; Masschaele, B.; Jacobs, P.J.S.; Van Acker, J. Detection and distribution analysis of organosilicon compounds in wood by means of SEM-EDX and micro-CT. *Mater. Charact.* **2006**, *56*, 39–48. [CrossRef]
3. Petrillo, M.; Sandak, J.; Grossi, P.; Sandak, A. Chemical and appearance changes of wood due to artificial weathering—Dose-response model. *J. Near Infrared Spectrosc.* **2019**, *27*, 26–37. [CrossRef]
4. Williams, R.R. Weathering of wood. In *Handbook of Wood Chemistry and Wood Composites*, 1st ed.; Rowell, R.M., Ed.; CRC Press: Boca Raton, FL, USA, 2005; pp. 139–185.
5. Low-Temperature EMMA®/EMMAQUA®. Available online: https://www.atlas-mts.com/products/accelerated-weathering-test-services/natural-weathering/accelerated-weathering-test/emmaqua-weathering-test (accessed on 3 January 2021).
6. Kennedy, R.W.; Ifju, G. Application of microtensile testing to thin wood sections. *Tappi* **1962**, *45*, 725–733.
7. Manwiller, F.G.; Godfrey, P.R. Microtensile strength of spruce pine after exposure to acids and bases. *Wood Sci.* **1973**, *5*, 295–297.
8. Raczkowski, J. Natural atmospheric corrosion of microtome wood sections. In Proceedings of the 10th Symp. on Wood Protection, Rogów, Poland, 17–19 October 1978. (In Polish).
9. Raczkowski, J. Seasonal effects on the atmospheric corrosion of spruce micro-sections. *Holz Roh Werkst.* **1980**, *38*, 231–234. [CrossRef]
10. *BS EN 927-6 Paints and Varnishes. Coating Materials and Coating Systems for Exterior Wood*; European Committee for Standardization: Brussels, Belgium, 2018.
11. Arnold, M.; Sell, J.; Feist, W.C. Wood weathering in fluorescent ultraviolet and xenon arc chambers. *For. Prod. J.* **1991**, *41*, 40–44.
12. Podgorski, L.; Arnold, M.; Hora, G. A reliable artificial weathering test for wood coatings. *Coat. World* **2003**, *2*, 39–48.
13. Grüll, G.; Tscherne, F.; Spitaler, I.; Forsthuber, B. Comparison of wood coating durability in natural weathering and artificial weathering using fluorescent UV-lamps and water. *Eur. J. Wood Prod.* **2014**, *72*, 367–376. [CrossRef]
14. Ozgenc, O. Comparing durability of wood material in natural and artificial weathering conditions. *ProLigno* **2016**, *12*, 3–11.
15. Rüther, P.; Jelle, B.P. Color changes of wood and wood-based materials due to natural and artificial weathering. *Wood Mater. Sci. Eng.* **2013**, *8*, 13–25.
16. Brischke, C.; Thelandersson, S. Modelling the outdoor performance of wood products—A review on existing approaches. *Constr. Build. Mater.* **2014**, *66*, 384–397. [CrossRef]
17. Rüther, P.; Time, B. External wood claddings—Performance criteria, driving rain and large-scale water penetration methods. *Wood Mater. Sci. Eng.* **2016**, *10*, 287–299. [CrossRef]
18. Thiis, T.K.; Burud, I.; Kranitis, D.; Gobakken, L.R. Simulation of surface climate and mould growth on wooden facades. In *The International Research Group on Wood Protection IRG/WP 16-20585*; IRG Secretariat: Stockholm, Sweden, 2016.
19. Sandak, J.; Sandak, A.; Riggio, M. Characterization and monitoring of surface weathering on exposed timber structures with multi-sensor approach. *Int. J. Archit. Herit.* **2015**, *9*, 674–688. [CrossRef]
20. Sandak, J.; Sandak, A.; Burud, I. Modelling of weathering. In *Performance of Bio-Based Building Materials*, 1st ed.; Jones, D., Brischke, C., Eds.; Woodhead Publishing: Cambridge, UK, 2017; pp. 502–510.
21. Salmén, L. Wood morphology and properties from molecular perspectives. *Ann. For. Sci.* **2015**, *72*, 679–684. [CrossRef]
22. Wiedenhoeft, A. Structure and function of wood. In *Wood Handbook: Wood as an Engineering Material*; Rowell, R.M., Ed.; Forest Products Laboratory: Madison, WI, USA, 2010; pp. 3.1–3.18.
23. Fengel, D.; Wegener, G. *Wood—Chemistry, Ultrastructure, Reactions*; Walter de Gruyter: New York, NY, USA, 1989.
24. Chinga-Carrasco, G.; Johnsen, P.O.; Øyaas, K. Structural quantification of wood fibre surfaces—Morphological effects of pulping and enzymatic treatment. *Micron* **2010**, *41*, 648–659. [CrossRef] [PubMed]
25. Hamed, S.A.M.; Ali, M.F.; El Hadidi, N.M.N. Using SEM in monitoring changes in archaeological wood: A review. In *Current Microscopy Contributions to Advances in Science and Technology*; Méndez-Vilas, A., Ed.; Formatex Research Center: Badajoz, Spain, 2012; pp. 1077–1084.
26. Jingran, G.; Jian, L.; Jian, Q.; Menglin, G. Degradation assessment of waterlogged wood at Haimenkou site. *Frat. Integrità Strutt.* **2014**, *30*, 495–501. [CrossRef]
27. Nicole, M.; Chamberland, H.; Rioux, D.; Xixuan, X.; Blanchette, R.A.; Geiger, J.P.; Ouellette, G.B. Wood degradation by Phellinus noxius: uItrastructure and cytochemistry. *Can. J. Microbiol.* **1995**, *41*, 253–265. [CrossRef]
28. Popescu, C.M.; Tibirna, C.M.; Nanoliu, A.; Gradinariu, P.; Vasile, C. Microscopic study of lime wood degraded by Chaetomium globosum. *Cellul. Chem. Technol.* **2011**, *45*, 565–569.
29. Singh, A.P.; Singh, T.; Rickard, C.L. Visualising impregnated chitosan in Pinus radiata early wood cells using light and scanning electron microscopy. *Micron* **2010**, *41*, 263–267. [CrossRef]
30. Singh, A.P.; Anderson, R.; Parka, B.D.; Nuryawana, A. A novel approach for FE-SEM imaging of wood-matrix polymer interface in a biocomposite. *Micron* **2013**, *54–55*, 87–90. [CrossRef] [PubMed]

31. Turkulin, H.; Arnold, M.; Derbyshire, H.; Sell, J. Structural and fractographic SEM analysis of exterior coated wood. *Surf. Coat. Int. Part B Coat. Trans.* **2001**, *84*, 67–75. [CrossRef]
32. Pfeffer, A.; Mai, C.; Militz, H. Weathering characteristics of wood treated with water glass, siloxane or DMDHEU. *Eur. J. Wood Prod.* **2012**, *70*, 165–176. [CrossRef]
33. Kocaefe, D.; Huang, X.; Kocaefe, Y. Comparison of weathering behaviours of heat-treated jack pine during different artificial weathering conditions. In Proceedings of the 4th International Conference on Fluid Mechanics and Heat & Mass Transfer (FLUIDSHEAT'13), Dubrovnik, Croatia, 25–27 June 2013; pp. 74–79.
34. Ganne-Chedeville, C.; Volkmer, T.; Letsch, B.; Lehmann, M. Measures for the maintenance of untreated wood facades. In Proceedings of the WCTE, Auckland, New Zealand, 15–19 July 2012; p. 6.
35. Fackler, K.; Schwanninger, M. How spectroscopy and microspectroscopy of degraded wood contribute to understand fungal wood decay. *Appl. Microbiol. Biotechnol.* **2012**, *96*, 587–599. [CrossRef]
36. Sandak, A.; Sandak, J.; Riggio, M. Assessment of wood structural members degradation by means of infrared spectroscopy: An overview. *Struct. Control Health* **2016**, *23*, 396–408. [CrossRef]
37. Popescu, C.M.; Popescu, M.C.; Vasile, C. Structural changes in biodegraded lime wood. *Carbohydr. Polym.* **2010**, *79*, 362–372. [CrossRef]
38. Popescu, C.M.; Froidevaux, J.; Navi, P.; Popescu, M.C. Structural modifications of Tilia cordata wood during heat treatment investigated by FT-IR and 2D IR correlation spectroscopy. *J. Mol. Struct.* **2013**, *1033*, 176–186. [CrossRef]
39. Huang, A.; Zhou, Q.; Liu, J.; Fei, B.; Sun, S. Distinction of three wood species by Fourier transform infrared spectroscopy and two-dimensional correlation IR spectroscopy. *J. Mol. Struct.* **2008**, *883*, 160–166. [CrossRef]
40. Sandak, A.; Sandak, J.; Burud, I.; Gobakken, L.R. Weathering kinetics of thin wood veneers assessed with near infrared spectroscopy. *J. Near Infrared Spectrosc.* **2016**, *24*, 549–553. [CrossRef]
41. Gallagher, N.B.; Blake, T.A.; Gassman, P.L. Application of extended inverse scatter correction to mid-infrared reflectance spectra of soil. *J. Chemometr.* **2005**, *19*, 271–281. [CrossRef]
42. Faix, O. Classification of lignins from different botanical origins by FT-IR spectroscopy. *Holzforschung* **1991**, *45*, 21–27. [CrossRef]
43. Schwanninger, M.; Rodrigues, J.; Pereira, H.; Hinterstoisser, B. Effects of short-time vibratory ball milling on the shape of FT-IR spectra of wood and cellulose. *Vib. Spectrosc.* **2004**, *36*, 23–40. [CrossRef]
44. Popescu, C.M.; Vasile, C.; Popescu, M.C. Degradation of lime wood painting supports II. Spectral characterisation. *Cellul. Chem. Technol.* **2006**, *40*, 649–658.
45. McLean, J.P.; Jin, G.; Brennan, M.; Nieuwoudt, M.K.; Harris, P.J. Using NIR and ATR-FTIR spectroscopy to rapidly detect compression wood in Pinus radiata. *Can. J. For. Res.* **2014**, *44*, 820–830. [CrossRef]
46. Guo, X.; Wu, Y.; Yan, N. In situ micro-FTIR observation of molecular association of adsorbed water with heat-treated wood. *Wood Sci. Technol.* **2018**, *52*, 971–985. [CrossRef]
47. Nejad, S.M.M.; Madhoushi, M.; Vakili, M.; Rasouli, D. Evaluation of degradation in chemical compounds of wood in historical buildings using FT-IR and FT-Raman vibrational spectroscopy. *Maderas Cienc. Tecnol.* **2019**, *21*, 381–392.
48. Noda, I.; Ozaki, Y. *Two-Dimensional Correlation Spectroscopy*; John Willey & Sons Ltd.: Chichester, UK, 2005.
49. Noda, I. Two-dimensional infrared spectroscopy. *J. Am. Chem. Soc.* **1989**, *111*, 8116–8118. [CrossRef]
50. Evans, P.D. Effect of angle of exposure on the weathering of wood surfaces. *Polym. Degrad. Stabil.* **1989**, *24*, 81–87. [CrossRef]
51. Cogulet, A.; Blanchet, P.; Landry, V. Wood degradation under UV irradiation: A lignin characterization. *J. Photochem. Photobiol. B* **2016**, *158*, 184–191. [CrossRef]
52. Kishino, M.; Nakano, T. Artificial weathering of tropical woods. Part1: Changes in wettability. *Holzforschung* **2004**, *58*, 552–557. [CrossRef]
53. *EN 927-3 Paints and Varnishes—Coating Materials and Coating Systems for Exterior Wood—Part 3: Natural Weathering Test*; European Committee for Standardization: Brussels, Belgium, 2000.
54. Müller, U.; Rätzsch, M.; Schwanninger, M.; Steiner, M.; Zöbl, H. Yellowing and IR-changes of spruce wood as result of UV-irradiation. *J. Photochem. Photobiol. B* **2003**, *69*, 97–105. [CrossRef]
55. Tolvaj, L.; Faix, O. Artificial ageing of wood monitored by DRIFT spectroscopy and CIE *L*a*b** colour measurements. *Holzforschung* **1995**, *45*, 397–404. [CrossRef]
56. Turkulin, H. *SEM Methods in Surface Research on Wood*; COST E 18 Final Seminar; CTBA: Paris, France, 2004.
57. Sandberg, D. Weathering of radial and tangential wood surfaces of pine and spruce. *Holzforschung* **1999**, *53*, 355–364. [CrossRef]
58. Pandley, K.K.; Pitman, A.J. Weathering characteristics of modified rubberwood (*Hevea brasiliensis*). *J. Appl. Polym. Sci.* **2002**, *85*, 622–631. [CrossRef]
59. Owen, J.A.; Owen, N.L.; Feist, W.C. Scanning electron microscope and infrared studies of weathering in southern pine. *J. Mol. Struct.* **1993**, *300*, 105–114. [CrossRef]
60. Timar, M.C.; Varodi, A.M.; Gurău, L. Comparative study of photodegradation of six wood species after short-time UV exposure. *Wood Sci. Technol.* **2016**, *50*, 135–163.
61. Noda, I. Advances in two-dimensional correlation spectroscopy (2DCOS). In *Frontiers and Advances in Molecular Spectroscopy*, 1st ed.; Laane, J., Ed.; Elsevier Science Publishing Co Inc.: Cambridge, MA, USA, 2017; pp. 47–75.
62. Grossman, D.M. Errors caused by using Joules to time laboratory and outdoor exposure tests. In *Accelerated and Outdoor Durability Testing of Organic Materials*; Grossman, D., Ketola, W., Eds.; ASTM International: West Conshohocken, PA, USA, 1994; pp. 68–87.

63. Burud, I.; Sandak, A.; Sandak, J.; Flö, A.; Thiis, T.; Gobakken, R.L.; Smeland, K.A.; Kvaal, K. Weather degradation of thin wood samples assessed with NIR hypersepctral imaging in transmission mode. In Proceedings of the 17th International Conference on Near Infrared Spectroscopy, Foz do Iguassu, Brazil, 18–23 October 2015; pp. 23–25.
64. Groves, K.W.; Banana, A.Y. Weathering characteristics of Australian grown radiata pine. *J. Inst. Wood Sci.* **1986**, *10*, 210–213.
65. Wang, Y.; Zhu, W.; Zhang, X.; Cai, G.; Wan, B. Influence of thickness on water absorption and tensile strength of BFRP Laminates in water or alkaline solution and a thickness-dependent accelerated ageing method for BFRP laminates. *Appl. Sci.* **2020**, *10*, 3618. [CrossRef]
66. Jelle, B.P. Accelerated climate ageing of building materials, components and structures in the laboratory. *J. Mater. Sci.* **2012**, *47*, 6475–6496.
67. Jankowska, A.; Rybak, K.; Nowacka, M.; Boruszewski, P. Insight of weathering processes based on monitoring surface characteristic of tropical wood species. *Coatings* **2020**, *10*, 877. [CrossRef]